Second Order Robust Regularization Cost Function for Detecting and Reconstructing Phase Discontinuities

Carlos Galvan[1] and Mariano Rivera[2]

[1]Centro Nacional de Metrologia

Apartado Postal 1-100 Centro, Queretaro, Queretaro, Mexico 76000

[1]cgalvan@cenam.mx,

[2]Centro de Investigacion en Matematicas A.C.

Apartado Postal 402, Guanajuato, Guanajuato, Mexico 36000

[2]mrivera@cimat.mx

Abstract. We propose a robust method for computing discontinuous phase maps from fringe pattern with carrier frequency. Our algorithm is based on the minimization of an edge-preserving regularized cost functional, specifically, on a robust regularized potential which uses the Plate with Adaptive Rest Condition paradigm (PARC), i.e. a second order edge preserving potential. Given that the proposed cost function is no-convex, our method uses as initial point an over smoothed phase computed with a standard fringe analysis method and then reconstructs the phase discontinuities. Although the method is for general purpose, it is introduced in the context of interferometric Gauge Blocks calibration. The performance of the algorithm is demonstrated by numerical experiments with both synthetic and real data. © Optical Society of America (OSA)

OCIS codes: 120.265, 0120.3180, 120.3940, 120.6650, 100.3190.

1. INTRODUCTION

The phase recovering from discontinuous fringe patterns is a challenging problem with relevant importance when phase stepping method are not applicable because of fast transient phenomena either of the studio object or illumination condition. In this paper we present a general algorithm for computing discontinuous phases and illumination component maps. Given that the proposed cost function is not quadratic our method uses as starting point the unwrapped phase[1,2] of the one computed with a standard fringe analysis algorithm (for instance the one proposed by Takeda et al.[3] or Womack[4]). Such an initial phase has phase discontinuities over smoothed and a residual tilt product of the remaining carrier frequency. The proposed method detects the phase discontinuities and reconstructs the discontinuous phase. Our algorithm can be applied to those cases where a good approximation of the discontinuous phase is available. In this sense our method is close related with phase refinement method recently reported by Rivera[5], however the in this paper we focus on the detection and reconstruction of phase discontinuities.

We use as studio case the observed interferograms in the Gauge Block (GB) calibration process[6,7,8]. The GB calibration task, by interferometric means, is performed by primary metrology laboratories. For instance, some of those laboratories are: the National Institute of Standards and Technology (NIST) in the United States of America, the National Research Council (NRC) in Canada, the National Physics Laboratory (NPL) in the UK, and the Centro Nacional de Metrologia (CENAM) in Mexico.

Calibration of GBs is the first step of the dissemination chain of the length standard: the meter; only this primary length standard is determined with higher precision than GBs. This highly precise calibration task is performed with optical interferometers (previously calibrated with respect to the primary length standard. The primary GBs, optically calibrated, are used as

standards for calibrating others GBs. That less precise secondary calibration is performed with mechanical comparators.

This paper concerns about GB calibration by interferometric techniques. Specifically, we present an algorithm for phase retrieval from a single interferogram of GBs. In figure 1, we show interferograms that corresponds to GBs of different material: Tungsten-carbide [Fig. 1(a)] and steel [Fig. 1(b)]. These fringe patterns were obtained from the video signal of the GB Interferometer of the CENAM. That explains the spurious column shift in the image. Such an interferometer is a commercial instrument based on a Twyman-Green setup with two different wavelength lasers beams: 633 nm and 540. The procedure for estimating the GB length is described by Pugh and Jackson[6] and it is briefly described follows. The GBs, to be measured, are wrung onto a lapped reference plate and positioned in the interferometer such that open fringes across the GB and plate are observed. The fringe pattern spatial frequency is controlled by a piezo-nano-actuator (PZT) that produces a tilt of the reference mirror. The GB introduces fringe displacements in the GB region with respect to the fringes in the plate region. Such relative fringe displacements are known as fringe fractions. A coarse measure of the GB length is computed from the relative phase between the interferograms corresponding to 633 nm and 543 nm wavelength. This GB length is computed with a limited precision: with an error between ± 1.5 μm with respect to the true length. In a second stage, the initial measure is improved with the high precision phase map computed from the interferogram corresponding to 543 nm (Fig. 1). Unfortunately, if one uses standard fringe analysis algorithms for estimating the correction phase map, then the phase discontinuity between the GB and the plate is over-smoothed; i.e. the correction phase map is corrupted. In this paper we present a fringe analysis method, for interferograms with frequency carrier, which recovers discontinuous phase maps; as the ones

shown in Fig. 1. Such interferograms can be represented by the observation model (or direct model):

$$g_r = \hat{a}_r + \hat{b}_r \cos(\hat{w}^T r + \hat{f}_r) + h_r, \tag{1}$$

where $r = [x, y]^T$ represents the position of the pixel r in the regular lattice L, $\hat{a}$ and $\hat{b}$ are the background and contrast illumination components, respectively; $\hat{w} = [\hat{w}_x, \hat{w}_y]^T$ is the spatial carrier frequency, $\hat{f}$ is the phase, and h represents independent additive noise introduced in the image at the acquisition time. The task is to compute an estimation f of the phase map $\hat{f}$ for each pixel of the fringe pattern. Based on prior knowledge of the experimental set-up, we can make the considerations stated in Table I.

Table I. Prior knowledge about the fringe pattern.

a)	The illumination components (background and contrast) are piecewise smooth because the elements in the image (reference plate and GB) may be composed of different materials.
b)	The phase is piecewise smooth because of the GB.
c)	The carrier frequency, $\hat{w}$, is constant, but its precise value is unknown. However a estimation, w, of the carrier can be computed. Moreover, the carrier frequency was chosen in a way such that an opened fringe interferogram is observed.

Prior knowledge in Table I needs (and must) be taken into account in order to effectively recover the phase, $\hat{f}$, from an interferogram of GB. For such a purpose, in last decade several authors

have proposed methods using regularization techniques[9] like: Quadrature filters[10], adaptive quadrature filters[11] or robust cost functions[5,12]. But those techniques neither consider the illumination components nor phase discontinuities in the analysis. Herein we propose a method for computing an estimation, f, of the fractional displacement of the fringe pattern in the GB calibration task, $\hat{f}$, given the fringe pattern, g, and a estimation of the carrier frequency, w. To solve such an inverse problem, we minimize a regularized cost function of the general form[13]:

$$U(a,b,f,l;g,w) = D(a,b,f;g,w) + l\,R(a,b,f,l), \tag{2}$$

where first term, *D*, is known as the data term and promotes fidelity of the computed variables to the observed data, i.e. the estimated phase and illumination components (f, a and b, respectively) should be consistent with the observed data, g, and the estimated frequency, w, according to model in Eq. (1). Note that we propose the joint estimation of the phase and the illumination components. Second term, *R*, codifies our *a priori* information about the solution, i.e. the *a priori* information expressed in Table I. Generally, the regularization term is expressed as a potential that promotes smooth solutions. Finally, the field l acts as a phase discontinuity indicator map. Given that the phase discontinuity locations are not known in advance, our method also estimates the edge detector field, *l*.

The paper is organized as follows. Section 2 presents a review of the regularization method based on the Plate with Adaptive Rest Condition paradigm[12] (PARC potentials). Such a method is a second order edge preserving regularization method that deals naturally with first and second order discontinuities: steps and slope breaks, respectively. Section 3 presents the method for the analysis of discontinuous fringe pattern. The method is based on the minimization of a regularized cost function with PARC potentials and it includes the joint estimation of the

illumination components. Section 4 shows experiments in both synthetic and real data that demonstrate the method performance. Finally, our conclusions are presented in section 5.

2. REGULARIZATION USING PARC POTENTIALS

Bayessian regularization, based on Markov Random Fields (MRF) theory[13], is a general and well accepted theoretical framework for solving inverse problems in image processing tasks. Such a theory has been effective to formulate algorithms for solving fringe analysis problems; for instance: fringes filtering[10,11],closed fringe analysis[5,14,15], phase unwrapping[1,2,16,17] and phase stepping[18,19]. In the MRF framework, the data term in Eq. (2) is formulated as a negative log-likelihood that depends on the observation model [Eq. (1)] and on the noise distribution[13]. Therefore, by assuming the noise, h, with identical independent Gaussian distribution, then the data term is expressed by:

$$D(a,b,f;g,w) = \sum_{r\in L} \left[g_r - a_r - b_r \cos\left(w^T r + f_r\right)\right]^2 . \tag{3}$$

On the other hand, the regularization term, R, must be expressed in a form such that imposes a penalty for violation the *prior* knowledge stated in Table I, section 1.

In order to choose the right form of the regularization term, we make the next consideration: robust regularized methods for image restoration based on first order potentials (i.e. in the adaptive membrane) promote flat (almost constant) reconstructions[12,20,21,22,23,24]. Those potentials are of the form:

$$R(f,l) = \sum_{\langle rs\rangle\in L} \left[(f_r - f_s)^2 l_{rs}^2 + \Phi(l_{rs})\right], \tag{4}$$

where the convex potential, $\Phi(\cdot)$, controls the discontinuities detection process and $\langle rs \rangle$ are cliques of first neighbor pixel pairs, i.e. $\langle rs \rangle = \{(r,s): |r-s| < 2\}$. It is well known that first order edge-preserving regularization potentials tend to sub-estimate slopes in the restored image. That produces a flatness of the slopes and introduces artificial edges in large slopes: The well-known staircase effect[12,21,25,26]. That is a limitation of first order edge-preserving regulatization potentials in fringe analysis because if the carrier frequency is estimated with a limited accuracy, then the residual carrier appears as a remaining constant slope in the phase. On the other hand, second order regularization terms (the thin plate model) are expressed as the summation of quadratic potentials. Such summation runs over cliques of pixels triads, $\langle qrs \rangle$, in horizontal, vertical and diagonal positions (see Fig. 2)[5]:

$$R(f) = \sum_{\langle qrs \rangle \in L} (f_q - 2f_r + f_s)^2 . \tag{5}$$

In spite of the quadratic potential (5) promotes smooth gradient solutions, this tends to over-smooth edges. That motivated to Geman and Reynolds to proposed the robust second order potentials[21],

$$R(f,l) = \sum_{\langle qrs \rangle \in L} \left[(f_q - 2f_r + f_s)^2 l_{qrs}^2 + \Phi(l_{qrs}) \right], \tag{6}$$

that preserves slope changes. However, it is well known that potential (6) over-smoothes steps in f. Recently, Rivera and Marroquin[12] proposed a new family of robust second order potential: the so-called plates with adaptive rest condition (PARC) potentials. PARC potentials can deal with ramps (regions with smooth variations in the intensity gradient) and first order

discontinuities (spatial steps). That is a significant advantage with respect to potentials based on the Geman and Reynolds' formulation. In this paper we implement the second order edge-preserving potentials with explicit line process[12] (PARC-EL). The PARC-EL based regularization term is expressed as a summation over cliques of size three of the form (see Fig. 2):

$$R_3(f,l) = \sum_{\langle rqs \rangle \in L} r_{qrs}(f,l), \tag{7}$$

with the PARC-EL potential, $r_{qrs}(f,l)$, defined by

$$r_{qrs}(f,l) = \left[l_{qr}\Delta f_{qr} - l_{rs}\Delta f_{rs}\right]^2 + m\left[(1-l_{qr})^2 + (1-l_{rs})^2\right]; \tag{8}$$

where we define $\Delta f_{qr} \overset{def}{=} f_q - f_r$, Δf_{rs} is defined in a similar way, and l_{rs} acts as a first and second order discontinuities detector; i.e. l_{rs} is close to zero if there is a step or an abrupt change in the f-slope between the first neighbor pixel pair $\langle r,s \rangle$.

The behavior of the PARC-EL potential is following explained. The contribution of the regularization term is computed as a compromise between the two terms in (8) which relative contributions are controlled by the positive parameter m; by depending of the values of the local differences, Δf_{qr} and Δf_{rs}, we have three cases:

a. Second order smoothness. If the thin plate potential is relatively small, $\left|\Delta f_{qr} - \Delta f_{rs}\right| < 2m$, then the minimum cost is achieved with $l_{qr} \approx 1$ and $l_{rs} \approx 1$. This implies the case of first order smoothness: $\left|\Delta f_{qr}\right| < m$ and $\left|\Delta f_{rs}\right| < m$.

b. Second order discontinuities preservation. For large plate potential values, $\left|\Delta f_{qr} - \Delta f_{rs}\right| > 2m$, with $\left|\Delta f_{qr}\right| > m$ and $\left|\Delta f_{rs}\right| > m$, the PARC-EL potential behaves as the Geman-Reynolds robust potential [Eq. (6)] and the minimum cost (close to $2m$) is achieved with $l_{qr} \approx 0$ and $l_{rs} \approx 0$.

c. First order discontinuities preservation. For $\left|\Delta f_{qr}\right| < m$ and $\left|\Delta f_{rs}\right| > m$, the PARC-EL potential becomes robust to the largest difference, i.e. the minimum potential cost is obtained with $l_{qr} \approx 1$ and $l_{rs} \approx 0$. For the case when $\left|\Delta f_{qr}\right| > m$ and $\left|\Delta f_{rs}\right| < m$, the PARC-EL potentials has a similar behavior and the minimum cost is obtained with $l_{qr} \approx 0$ and $l_{rs} \approx 1$.

Next section presents the complete functional for phase recovery with second order discontinuities.

3. EDGE PRESERVING FUNCTIONAL FOR FRINGE ANALYSIS BASED ON PARC-EL POTENTIALS

The carrier frequency, $\hat{w} = \left[\hat{w}_x, \hat{w}_y\right]^T$ in model (1), can be estimated with a limited precision. Because such a residual error, standard fringe analysis methods[3,4] introduce a constant slope in the recovered (estimated) phase, f^0. Moreover, given that the mentioned standard fringe analysis algorithms (Takeda et al. [3] and Womack[4]) assume limited bandwidth phases (smooth phases)

then the real phase discontinuities will be over smoothed. In this work we proposed to use the f^0 as an initial phase (starting point) and then to detect and reconstruct the phase discontinuities. For such a purpose we use PARC-EL potentials in the regularization term, *R*: to recover piecewise smooth-sloped phase maps. Moreover, we assume that illumination components discontinuities coincide with phase discontinuities (see Fig. 1). So that, phase and illumination steps are coupled in the PARC-EL potential by a unique edge detector field, *l*. Therefore, we propose to compute the phase and the illumination components minimizing the cost function:

$$\begin{aligned} U(a,b,f,l) = & \sum_{r\in L}\left[g_r - a_r - b_r\cos\left(w^T r + f_r\right)\right]^2 \\ & + \sum_{\langle q,r,s\rangle\in L}\left\{l_a\left(l_{qr}\Delta a_{qr} - l_{rs}\Delta a_{rs}\right)^2 + l_b\left(l_{qr}\Delta b_{qr} - l_{rs}\Delta b_{rs}\right)^2\right. \\ & \left. + l_c\left(l_{qr}\Delta f_{qr} - l_{rs}\Delta f_{rs}\right)^2 + m\left[(1-l_{qr})^2 + (1-l_{rs})^2\right]\right\}, \end{aligned} \tag{9}$$

where the positive regularization parameters, l_a, l_b, l_c, and m, control the relative contribution of each term to the total cost. The minimization, of (9), is performed by alternating minimizations with respect to f, a, b and l; such a scheme consists of iterating until convergence the Algorithm for analysis of discontinuous fringe patterns (ADFP).

ADFP Algorithm.

---

1. Choose l_a, l_b, l_c and m;
2. Compute an approximation of the carrier frequency, $w = [w_x, w_y]^T$;
3. Set $a_r^0 = 1$, $b_r^0 = 1$ and $l_r^0 = 1$ for all $r \in L$;
4. Compute an initial phase, f_r^0 for all $r \in L$; {*By using a standard fringe analysis method*[3,4] *and then by unwrapping the computed phase*[1,2].}

5. **for** $k = 0, 1, ...$

6. Compute $f^{k+1} = \arg\min_{f} U\left(a^k, b^k, f, l^k\right)$, using as initial guess $f = f^k$;

7. Compute $a^{k+1} = \arg\min_{a} U\left(a, b^k, f^{k+1}, l^k\right)$;

8. Compute $b^{k+1} = \arg\min_{b} U\left(a^{k+1}, b, f^{k+1}, l^k\right)$;

9. Compute $l^{k+1} = \arg\min_{l} U\left(a^{k+1}, b^{k+1}, f^{k+1}, l\right)$;

10. **if** $\left\| f^k - f^{k-1} \right\|_2^2 < e$

11. **STOP**, with solution $\left(a^{k+1}, b^{k+1}, f^{k+1}, l^{k+1}\right)$;

12. **end for**

In this work we compute an estimation, $w = \left[w_x, w_y\right]^T$, of the fringe pattern carrier frequency with the method reported by Huntley[27]. Note that, because of the cosine function, the minimization with respect to (w.r.t.) the phase f^{k+1} (step 1 of ADFP algorithm) leads us to the solution of a non-linear equation system. For solving such a non-linear system we use simple gradient descent algorithm that uses as starting point the result of the previous step, f^k, i.e. by assuming fixed a^k, b^k and l^k, then f^{k+1} is computed as the fixed point of the gradient descent iteration:

$$f_{t+1}^{k+1} = f_t^{k+1} - a \nabla_f U\left(a^k, b^k, f_t^{k+1}, l^k\right); \tag{10}$$

where a is the step size, $f_0^{k+1} = f^k$ is the initial guess and $\nabla_f U\left(a^k, b^k, f_t^{k+1}, l^k\right)$ denotes the partial gradient of the cost function U w.r.t. the phase f and evaluated at f_t^{k+1}. The initial phase, f^0, is be computed with a standard spatial fringe analysis algorithm[4,28]. We noted that if the initial phase is a homogeneous map equal to 0, the ADFP algorithm computes a wrapped phase, i.e. discontinuities (edges) are inroduced at those sites where the phase is wrapped. Additionally, steps 2, 3 and 4 (in the ADFP algorithm) correspond to perform quadratic minimizations, i.e. to solve the linear systems: $\nabla_a U\left(a, b^k, f_t^{k+1}, l^k\right) = 0$, $\nabla_b U\left(a^{k+1}, b, f_t^{k+1}, l^k\right) = 0$, and $\nabla_l U\left(a^{k+1}, b^{k+1}, f_t^{k+1}, l\right) = 0$, respectively. Such minimizations can be achieved with standard fast minimization algorithms as a Gauss-Seidel scheme or the conjugate gradient[29]. More details of the procedure for computing the discontinuities detector field, l, are given in the Appendix A.

ADFP algorithm requires us to find the exact partial minimization and therefore it is computationally inefficient. However, in practice, such partial minimizations are not fully achieved, but approximated in a way such that:

$$U\left(a^k, b^k, f^k, l^k\right) \geq U\left(a^k, b^k, f^{k+1}, l^k\right) \geq U\left(a^{k+1}, b^k, f^{k+1}, l^k\right) \geq U\left(a^{k+1}, b^{k+1}, f^{k+1}, l^k\right) \geq U\left(a^{k+1}, b^{k+1}, f^{k+1}, l^{k+1}\right) \geq 0$$

is satisfied at each iteration. The convergence to, at least, a local minimum is guaranteed because $U(a,b,f,l)$ is bounded by zero.

5. EXPERIMENTS

This section shows the results computed with the proposed ADFP algorithm in both synthetic and real data.

The first experiment corresponds to the analysis of one-dimensional synthetic data. Figure 3(a) shows the synthetic data (values of phase and illumination elements *a* and *b*) generated with the direct observation model [see Eq. (1)] and setting:

$$a_r = \{0.6 \;\; if \;\; 97 \le r \le 165, \quad 1.0 \;\; otherwise\},$$

$$b_r = \{0.5 \;\; if \;\; 97 \le r \le 165, \quad 0.9 \;\; otherwise\},$$

and

$$f_r = \{1.2 + 0.005r \;\; if \;\; 97 \le r \le 165, \quad 0.2 + 0.005r \;\; otherwise\}.$$

Then, the one-dimensional fringe pattern was generated using a known frequency, w, and corrupted with additive Gaussian noise. The experiments were performed using the real carrier frequencies; however, the phase has a small slope that simulates a residual carrier. Figure 3(b) shows the results computed by using the no-robust thin plate potential, Eq. (5): Note the over-smoothness of the phase and the steps in the illumination components. Figure 3(c) shows the results computed by using first order edge-preserving potentials and coupling edges of phase and the illumination components, i.e. Eq. (4) with $\Phi(l_{rs}) = m(1-l_{rs})^2$ and the parameter $m = 0.001$ for controlling the edge detection sensibility. In spite of discontinuities and illumination components are correctly computed, one can note that the phase slopes are sub-estimated. It is also well known that first order edge-preserving potentials introduce spurious edges in large slopes (a staircase effect). Panel (d) shows results computed with the proposed method. Table II shows the L_2-norm of the error vector of the phase and the illumination components computed by using different regularization potentials in Eq. (9): thin plate [Eq. (4)], robust membrane [Eq.

(5)] and PARC-EL [Eqs. (7) and (8)]. In spite of the robust membrane potential computes accurate illumination components (piecewise constant) the phase slope is underestimated. The best phase map (with piecewise smooth gradient) is computed with PARC-EL potentials. Last row in Table II shows the computational times for the compared regularized cost functions. We note, as expected, an extra computational cost of the PARC-EL formulation w.r.t. the Quadratic Plate based formulation but such a computational cost is not significantly if we take into account the phase improvement. Moreover such a computational times can be reduces if, instead of a low efficient simple gradient descent scheme [see (10)], one uses a more efficient minimization algorithms as the Newton or Gauss-Newton ones[29].

Table II. L_2 error of results and computational times computed with different potentials.

	Thin Plate (Quadratic)	Robust Membrane (Half-Quadratic)	Robust Thin Plate (PARC-EL)
Phase (f)	**4.9819**	**1.8936**	**0.9952**
Background (a)	0.4447	0.7123	0.5156
Contrast (b)	0.5122	0.6959	0.7704
Computational time (secs.)	40	25	51

Figure 4 shows the results computed from one-dimension real data. In this experiment a tungsten-carbide GB was wrung on a steel reference plate and the interferogram was acquired with the TESA Gauge Block Interferometer at CENAM. The results, showed in Fig. 4(b), show steps (discontinuities) in the phase (doted line) and in the illumination components (continuous

lines). One can observe a small tilt in the computed phase map in the GB region: Such a tilt may result from an incorrect wrung process of the GB on the reference plate. One can also note that the edges are not well defined in the data [Fig. 4(a)] and as consequence sharp discontinuities are not detected, see Fig. 4(b). The quality of such results can be improved by the two-dimensional processing of the fringe pattern.

Figure 5 shows the components computed with the proposed method in the two-dimensional fringe pattern showed in Fig 1(a). Figure 5(a) shows the piecewise phase map with the relative fractional phase between the GB and the reference plate. Figures 5(b) and 5(c) show the background and the contrast components, respectively. Finally, figure 5(d) shows the discontinuities map (edges). In this case, the computed discontinuities are sharp and located according with the observed edges in the noisy interferogram [in Fig. 1(a)]. The data were not preprocessed for reducing the noise or correcting the spurious column shift in the image.

6. CONCLUSIONS

We presented a regularization model for analysis of interferogram with discontinuities. The method estimates the phase map and the illumination components according with the interference equation.

The presented algorithm is a method for detect and reconstruct the spatial phase discontinuities provided an initial phase previously computed with a standard method. So that, in principle, if an over-smoothed discontinuities phase can be computed from a fringe pattern with (or without) carrier then our algorithm can be used for detect and restore such phase discontinuities. However, in general, the problem of close fringe analysis is beyond the scope of the proposed method (the reader can see Ref. 5 for more details about a method addressing such a problem).

Our algorithm uses as initial data the unwrapped phase computed with a standard fringe analysis algorithm. Given that such standard algorithms[3,4] assume smoothes (limited bandwidth) phase and illumination components the initial phase has over smoothed phase discontinuities. We assume that the discontinuity locations are not known in advance and so that they need to be estimated. The proposed method effectively detects and reconstructs the phase discontinuities. The presented ADFP algorithm is based on the minimization of a cost function that uses, as regularization potentials, thin plate potentials with adaptive rest condition, PARC potentials. PARC potentials constrain the solution to be piecewise with almost constant slopes. PARC potentials allow to recover discontinuous phase maps with piecewise smooth gradients, so that they are particularly useful when the carrier frequency is estimated with limited accuracy, so that a residual constant slope remains in the initial phase.

ACKNOWLEDGEMENTS

This work was partially done by C. Galvan as Master Thesis at the Centro de Investigacion en Matematicas and supported in part by a scholarship by the Consejo Nacional de Ciencia y Tecnologia (CONACYT) and a grant from the Centro Nacional de Metrología (CENAM), Mexico. M. Rivera was partially supported by the CONACYT under grant 40722 and 46270. The authors thank to the anonymous referees for their comments that help to improve the quality of the paper.

APPENDIX A. GAUSS-SEIDEL SCHEME FOR COMPUTING THE DISCONTINUITIES DETECTOR FIELD.

The one-dimensional (1D) case of the algorithm for computing the discontinuities detection field (step 9 in the ADFP algorithm) is presented. However this method can straightforward be extended to the two-dimensional case. Let $a, b, f \in \Re^N$ and $l \in \Re^{N-1}$, then we define: $\Delta x_i \stackrel{def}{=} x_i - x_{i-1}$, for $i = 1, 2, ..., N$. Therefore the 1D version of the cost function (9) is written as

$$U_{1d}(a, b, f, l) = Q(a, b, f) + \sum_{i=2}^{N-1} \{ l_a (l_i \Delta a_i - l_{i-1} \Delta a_{i-1})^2 + l_b (l_i \Delta b_i - l_{i-1} \Delta b_{i-1})^2 + l_c (l_i \Delta f_i - l_{i-1} \Delta f_{i-1})^2 + m [(1 - l_i)^2 + (1 - l_{i-1})^2] \},$$

where $Q(a,b,f)$ represents the independent terms of l. Then from

$$\frac{1}{2} \frac{\partial U_{1d}(a,b,f,l)}{\partial l_i} = 0,$$

we have

$$\begin{aligned} & l_a \Delta a_i [(l_i \Delta a_i - l_{i+1} \Delta a_{i+1}) W(i+1) + l_a (l_i \Delta a_i - l_{i-1} \Delta a_{i-1})] \\ & + l_b \Delta b_i [(l_i \Delta b_i - l_{i+1} \Delta b_{i+1}) W(i+1) + l_b (l_i \Delta b_i - l_{i-1} \Delta b_{i-1})] \\ & + l_c \Delta f_i [(l_i \Delta f_i - l_{i+1} \Delta f_{i+1}) W(i+1) + l_c (l_i \Delta f_i - l_{i-1} \Delta f_{i-1})] + m(l_i - 1) = 0; \end{aligned} \quad (11)$$

where $W(x) = \{1 \ if \ \ x < N-1; 0 \ otherwise\}$. The Gauss-Seidel scheme corresponds to solve (11) for l_i, keeping fixed a, b, f and (l_{i+1}, l_{i-1}), for $i = 2, 3, ..., N$; where l_{i-1} is the previously updated value. Such procedure is iterated for all the pixels until convergence. Note that the edge detector variable l_i is associated to the pair of pixels in the clique $\langle i, i-1 \rangle$.

References

1. J.L. Marroquin and M. Rivera, "Quadratic regularization functionals for phase unwrapping," J. Opt. Soc. Am. A, 12, 2393-2400 (1995).
2. M. Rivera, J.L. Marroquin, M. Servin and R. Rodriguez-Vera, "Fast algorithm for integrating inconsistent gradient fields," Appl. Opt. 36, 8381-8390 (1997).
3. M. Takeda, H. Ina, and S. Kobayashi, "Fourier–transform method of fringe-pattern analysis for computed-based topography and interferometry," J. Opt. Soc. Am., 4, 156-160 (1982).
4. K. H. Womack, "Interferometric phase measurement using spatial synchronous detection," Opt. Eng. (Bellingham) 23, 391-395 (1984).
5. M. Rivera, "Robust phase demodulation of interferograms with open or closed fringes," J. Opt. Soc. Am. A, J. Opt. Soc. Am. A, 22, 6, 1170-1175 (2005).
6. D. J. Pugh and K. Jackson, "Automatic gauge block measurement using multiple wavelength interferometer," in *Contemporary Optical Instrument Design, Fabrication and Testing*, H. Beckmann, J. Briers and P. R. Yoder, eds., in Proc. SPIE 0656, 233-250 (1986) .
7. G. Boensch, "Gauge blocks as length standards measured by interferometry or comparison: length definition, traceability chain, and limitations," in *Recent Developments in Optical Gauge Block Metrology*, J. E. Decker, N. Brown, eds., Proc. SPIE 3477 , 199-210 (1998)
8. G. Boensch, "Automatic gauge block measurement by phase stepping interferometry with three laser wavelengths," in *Recent Developments in Traceable Dimensional Measurements*, Jennifer E. Decker, Nicholas Brown, eds., Proc. SPIE 4401, 1-10 (2001).
9. J. L. Marroquin, M. Rivera, S. Botello, R. Rodriguez-Vera and M. Servin, "Regularization methods for processing fringe-pattern images," Appl. Opt. 38, 788-795 (1999).

10. J. L. Marroquin, J. E. Figueroa and M. Servin, "Robust quadrature filter," J. Opt. Soc. Am. A 14, 779-791 (1997).
11. J. L. Marroquin, M. Servin and R. Rodriguez-Vera, "Adaptive quadrature filters for multi-phase stepping images," Opt. Let. 23, 238-240 (1998).
12. M. Rivera and J. L. Marroquin, "Adaptive rest condition potentials: first and second order edge-preserving regularization," Journal of Computer Vision and Image Understanding, 88, 76-93 (2002).
13. J. L. Marroquin, S. Mitter and T. Poggio, "Probabilistic Solution of Ill-Posed Problems in Computational Vision," Journal of the American Statistical Association, 82, 76-89 (1987).
14. J. Villa, J. A. Quiroga and M. Servin, "Improved regularized phase tracking technique for the processing of squared-grating deflectograms," Appl. Opt. 39, 502–508 (2000).
15. R. Legarda-Saenz, W. Osten and W. Juptner, "Improvement of the Regularized Phase Tracking Technique for the Processing of Nonnormalized Fringe Patterns," Appl. Opt. 41, 5519-5526 (2002).
16. M. Rivera and J.L. Marroquin, "Half-quadratic cost functions for phase unwrapping," Optics Letters, 29, 504-506 (2004).
17. M. Servin, J. L. Marroquin, D. Malacara and F.J. Cuevas, "Phase unwrapping using a regularized phase tracking system", Appl. Opt. 37, 1917-1923 (1998).
18. J. L. Marroquin, M. Servin and R. Rodriguez-Vera, "Adaptive quadrature filters for multi--phase stepping images," Opt. Let. 23, 238-240 (1998).
19. M. Rivera, J. L. Marroquin, S. Botello and M. Servin, "A robust spatio-temporal quadrature filter for multi-phase stepping," Appl. Opt. 39, 284-292 (2000).

20. S. Geman and D. E. McClure, “Bayesian image analysis methods: An application to single photon emission tomography,” in Proc. Statistical Computation Section, Amer. Statistical Assoc., Washington, DC, 12–18 (1985)
21. D. Geman and G. Reynolds, “Constrained restoration and recovery of Discontinuities,” IEEE Trans. Pattern Analysis and machine Vision. 14, 367-383 (1992).
22. D. Geman and C. Yang, “Nonlinear image recovery with half-quadratic regularization,” IEEE Trans. Image Process. 4, 932–946, (1995).
23. M. J. Black and A. Rangarajan, “Unification of line process, outlier rejection, and robust statistics with application in early vision,” Int. Journal of Computer Vision, 19, 57–91 (1996).
24. M. Rivera and J.L. Marroquin, "Efficient half-quadratic regularization with granularity control," Journal of Image and Vision Computing, 21, 345-357 (2003).
25. M. Proesmans, A. E. Pouwels and L. Van Gool, “Couple geometry-driven diffusion equations for low level vision,” In Geometry-Driven Diffusion in Computer Vision, B. M. ter Haar-Romeny, Editors, 191–228, Kluwer Academic Publisher B.V. (1994).
26. T. Tasdizen and R. Withaker, “Feature preserving variational smoothing of terrain data,” in Proc. II IEEE Workshop on Variational, Geometric and Level Set Methods in Computer Vision (VLSM’03), 121-128 (2003).
27. J.M. Huntley, “An image processing system for the analysis of speckle photographs”, J. of Physics E: Sci. Instrum., 19, 43-49 (1986).
28. K. J. Gasvik, *Optical Metrology* (John Wiley & Sons, Inc. 3rd edition, Indianapolis, 2002).
29. J. Nocedal and S. Wright, *Numerical Optimization* (Springer Series in Operational Research, Springer-Verlag, New York, 1999).

List of Figure Captions

1. Interferograms of GB on a steel plate: a) Tungsten carbide and b) steel.

2. Cliques of pixels in positions: (a) horizontal, (b) vertical and (c) and (d) diagonal.

3. (a) Synthetic one dimensional data: Phase (continuous line), background (point-dash line) and contrast (pointed line). Computed results with: b) Quadratic thin plate potential, c) robust membrane potential, and d) PARC potential. The original data were corrupted with a white noise signal with mean equal zero and standard deviation of 0.5 radians.

4. Real data from TESA interferometer. a) Central column of the interferogram in Fig. 1(a), b) Computed results with the proposed ADFP algorithm: Phase (doted line), illumination components (solid lines) and edges (makers).

5. Two dimension fringe pattern analysis with the proposed ADFP algorithm: a) Phase map, b) background illumination, c) contrast component and d) detected edge map.

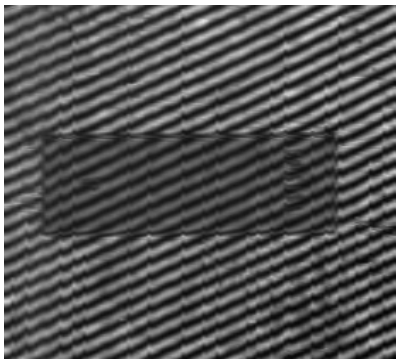

(a)

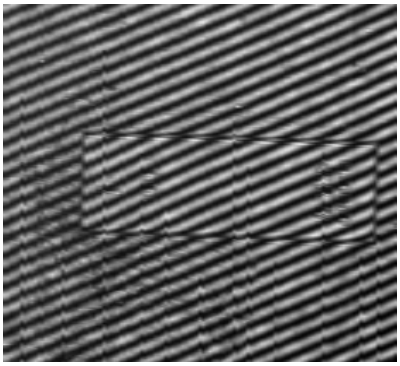

(b)

Fig. 1.

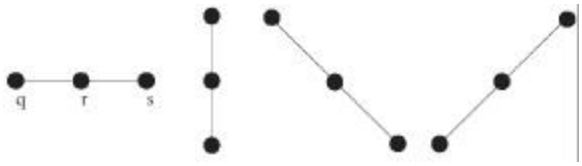

Fig. 2.

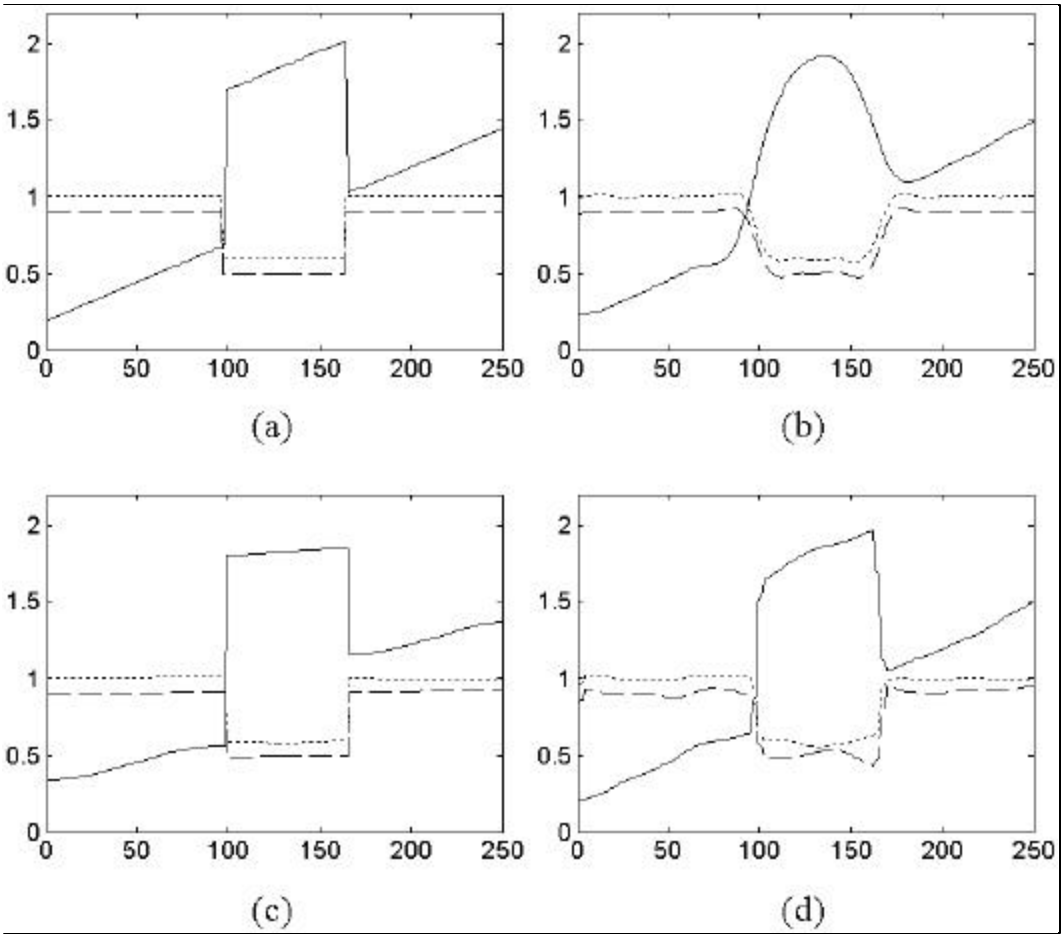

Fig 3.

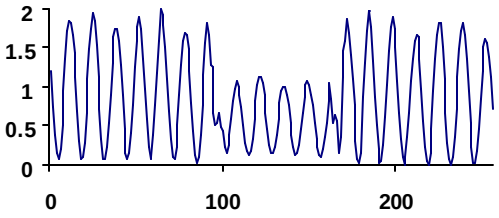

(a)

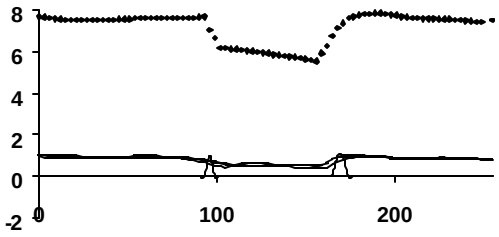

(b)

Fig 4.

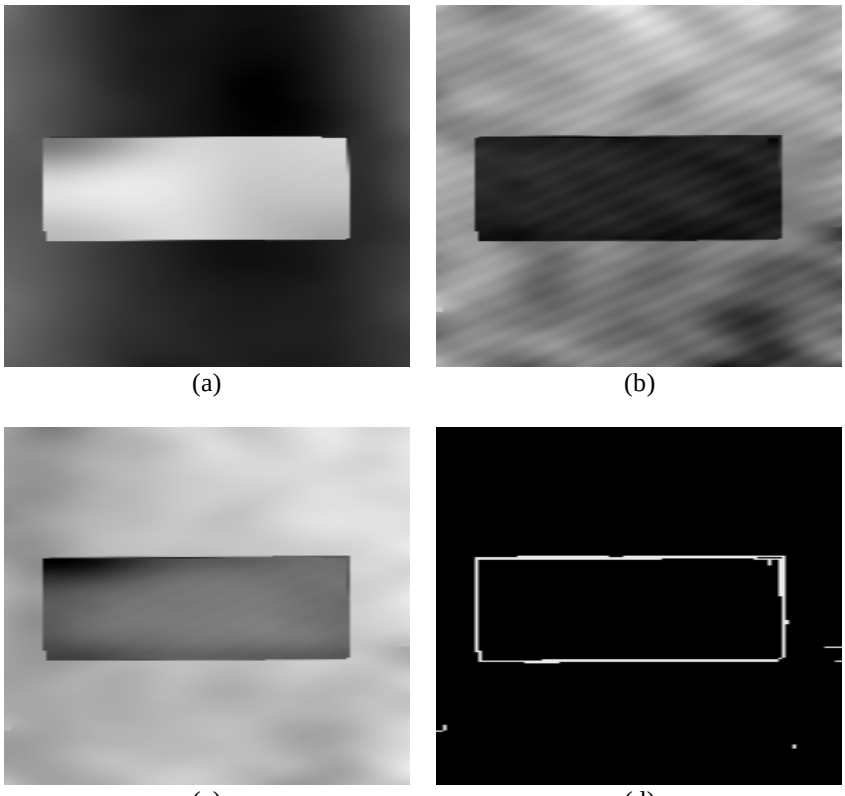

(a) (b)

(c) (d)

Fig 5.